Modelling non-ideal bio-physical-chemical effects on high-solids anaerobic digestion of the organic fraction of municipal solid waste

Vicente Pastor-Poquet, Stefano Papirio, Jean-Philippe Steyer, Eric Trably, Renaud Escudié, Giovanni Esposito

Modelling Non-Ideal Bio-Physical-Chemical Effects on High-Solids Anaerobic Digestion of the Organic Fraction of Municipal Solid Waste

Vicente Pastor-Poquet [a,b,*], Stefano Papirio [c], Jean-Philippe Steyer [b], Eric Trably [b], Renaud Escudié [b], and Giovanni Esposito [a]

[a] Department of Civil and Mechanical Engineering, University of Cassino and Southern Lazio, via Di Biasio 43, 03043 Cassino (FR), Italy

* Corresponding author. E-mail: vicente.pastor.poquet@gmail.com

[b] LBE, Univ Montpellier, INRA, 102 avenue des Etangs, 11100, Narbonne, France

[c] Department of Civil, Architectural and Environmental Engineering, University of Napoli Federico II, via Claudio 21, 80125 Napoli, Italy

ABSTRACT

This study evaluates the main effects of including 'non-ideal' bio-physical-chemical corrections in high-solids anaerobic digestion (HS-AD) of the organic fraction of municipal solid waste (OFMSW), at total solid (TS) between 10 and 40 %. As a novel approach, a simple 'non-ideal' module, accounting for the effects of ionic strength (*I*) on the main acid-base equilibriums, was coupled to a HS-AD model, to jointly evaluate the effects of 'non-ideality' and the TS content dynamics on the HS-AD bio-physical-chemistry. 'Non-ideality' influenced the pH, concentration of inhibitors (i.e. NH_3), and liquid-gas transfer (i.e. CO_2), particularly at higher TS (i.e. ≥ 20 %). Meanwhile, fitting the experimental data for batch assays at 15 % TS showed that HS-AD of OFMSW

might be operated at $I \geq 0.5$ M. Therefore, all HS-AD simulations should account for 'non-ideal' corrections, when assessing the main inhibitory mechanisms (i.e. NH_3 buildup and acidification) potentially occurring in HS-AD of OFMSW.

Keywords: High-Solids Anaerobic Digestion Model; Non-Ideal Bio-Physical-Chemical Corrections; Ionic Strength; Total Solids Dynamics; Ammonia Inhibition.

1 INTRODUCTION

Anaerobic digestion (AD) models enhance our understanding about the biogas production dynamics and/or inhibitory mechanisms, while revealing potential opportunities for bioprocess optimization (Lauwers et al., 2013; Steyer et al., 2006). The Anaerobic Digestion Model No.1 (ADM1) is a structured model reproducing the main bio-physical-chemical mechanisms in AD (Batstone et al., 2002). Biochemical mechanisms include the disintegration, hydrolysis, acidogenesis, acetogenesis and methanogenesis of organic substrates, expressed in chemical oxygen demand (COD) units. Physical-chemical mechanisms include the liquid-gas transfer of CH_4, CO_2 and H_2, and the ionic equilibriums of volatile fatty acids (VFA; i.e. acetic, propionic, butyric and valeric), inorganic nitrogen (i.e. NH_3), and inorganic carbon (i.e. CO_2).

High-solids anaerobic digestion (HS-AD) is operated at total solid (TS) content ≥ 10 %, in contrast to 'wet' AD (i.e. TS < 10 %) (Pastor-Poquet et al., 2019a). In HS-AD of the organic fraction of municipal solid waste (OFMSW), a 30 - 80 % volatile solid (VS) removal occurs due to the biogas production, modifying the reactor content mass

(M_{Global}) and/or volume (V_{Global}), but also the reactor content specific weight (ρ_{Global}) (Kayhanian & Tchobanoglous, 1996; Pastor-Poquet et al., 2018).

To account for the mass removal in HS-AD simulations, a HS-AD model based on ADM1 was developed (Pastor-Poquet et al., 2018). The main difference between the HS-AD model and the continuously-stirred tank reactor (CSTR) implementation of ADM1 (Batstone et al., 2002) lies on the simulation of the M_{Global}, V_{Global}, TS, VS, and ρ_{Global} dynamics by using an extended set of mass balances for homogenized HS-AD reactors. For example, apart from the mass balance of soluble ("S") and particulate ("X") substances in ADM1, the HS-AD model includes the mass balance of reactor mass (M_{Global}), solvent ($M_{Solvent}$), and inert (M_{Inerts}) contents, allowing the dynamic calculation of TS and VS. On the other hand, apparent concentrations (i.e. kg COD/m^3 Solvent) were used in the bio-physical-chemical framework of the HS-AD model, to account for the TS concentration effect on HS-AD solutes (i.e. VFA), and in contrast to ADM1 that uses global concentrations (i.e. kg COD/m^3 Total).

An important limitation of the physical-chemical framework of ADM1 is the absence of corrections for the 'non-ideal' solution effects on AD (Batstone et al., 2012; Solon et al., 2015; Tait et al., 2012). In solution, a global species concentration ($S_{T,i}$) includes the corresponding dissociated (S_i^{Zi}) and un-dissociated ($S_i^{Zi=0}$) species concentrations, with their associated ion charge (Z_i). Thus, the 'ideal' dissociated/un-dissociated species can be obtained from $S_{T,i}$ once knowing the mass balance, the 'ideal' equilibrium constant ($K_{a,i}$), and the solution pH. For example, the total ammonia/inorganic nitrogen (TAN, S_{in}) in AD is mainly dissociated into ammonium ion (NH_4^+, S_{nh4+}) and free ammonia

(NH_3, S_{nh3}), as a function of the equilibrium constant for inorganic nitrogen ($K_{a,in}$) and the proton concentration (H^+, S_{h+}) [Equation 1]. Using the inorganic nitrogen mass balance [Equation 2] and the 'ideal' ammonia equilibrium [Equation 3], S_{nh4+} and S_{nh3} can be approximated for a given pH – S_{h+} concentration.

$$NH_4^+ \overset{K_{a,in}}{\longleftrightarrow} NH_3 + H^+ \quad (1)$$

$$S_{in} = S_{nh_4{}^+} + S_{nh_3} \quad (2)$$

$$K_{a,in} = \frac{S_{nh_3} \cdot S_{h^+}}{S_{nh_4{}^+}} \quad (3)$$

Ionic strength (*I*) estimates the level of ionic interactions of an aqueous solution, and can be approximated from S_i^{Zi} and Z_i [Equation 4] (Parkhurst & Appelo, 1999; Solon et al., 2015). Whether a solution is not infinitely diluted (i.e. $\Sigma S_i^{Zi} \neq 0$), the hypothesis of 'ideality' (i.e. $I \sim 0$) is not further valid, and all the 'non-ideal' equilibriums involved in the solution must be expressed in terms of activities, instead of molal concentrations (Batstone et al., 2012; Tait et al., 2012). The activity of a solute (a_i) is the product of the molal concentration (S_i^{Zi}, kmol/kg Solvent) by the coefficient of activity (γ_i) [Equation 5]. 'Non-ideality' corrections are required for AD solutions when $I \geq 0.2$ M, being potentially important in HS-AD due to the high organic concentration used (Batstone et al., 2015; Solon et al., 2015; Tait et al., 2012).

$$I = \frac{1}{2}\sum {S_i}^{Z_i} \cdot {Z_i}^2 \quad (4)$$

$$a_i = \gamma_i \cdot {S_i}^{Z_i} \quad (5)$$

For an 'ideal' solution $\gamma_i = 1$, whereas for a 'non-ideal' solution $\gamma_i < 1$ for dissociate species (i.e. $Z_i \neq 0$) and $\gamma_i > 1$ for un-dissociated species (i.e. $Z_i = 0$). Thus, γ_i is mainly a function of I and, for a moderately concentrated solution (i.e. $I \leq 0.2$ M), the Davies equation [Equation 6] is commonly used for assessing the activity of ionic species (Allison et al., 1991; Parkhurst & Appelo, 1999). However, when $I > 0.2$ M, γ_i tends to unity with increasing I by using the Davies equation (Solon, 2016; Tait et al., 2012). Therefore, the WATEQ Debye-Hückel equation [Equation 7] is recommended for $0.2 \leq I \leq 1.0$ M, as γ_i progressively tends to zero with increasing I (Parkhurst & Appelo, 1999; Solon et al., 2015).

$$log_{10}(\gamma_i) = -A \cdot {Z_i}^2 \cdot \left(\frac{\sqrt{I}}{1+\sqrt{I}} - 0.3 \cdot I\right) \quad (6)$$

$$log_{10}(\gamma_i) = -\frac{A \cdot {Z_i}^2 \cdot \sqrt{I}}{1 + B \cdot a_i^0 \cdot \sqrt{I}} + b_i \cdot I \quad (7)$$

The liquid-gas transfer, ionic speciation, ion pairing and precipitation are the most important physical-chemical mechanisms affecting and being affected by 'non-ideality' in AD (Batstone et al., 2015; Flores-Alsina et al., 2015). In particular, the ionic speciation determines the medium pH, as well as the concentration of soluble inhibitors (i.e. NH_3), being two of the most important parameters influencing the biogas production in ADM1 (Batstone et al., 2002; Rosén & Jeppsson, 2006; Xu et al., 2015). Therefore, failing to include 'non-ideal' corrections in ADM1-based models might result in an artificially high NH_3 concentration, subsequently influencing the parameter calibration related to NH_3 inhibition (Hafner & Bisogni, 2009; Nielsen et al., 2008; Patón et al., 2018).

With all the above, the 'non-ideal' approach may be particularly important to assess the main inhibitory mechanisms in HS-AD of OFMSW, since HS-AD is easily subjected to reactor inhibition by high levels of NH_3, as a consequence of the high protein content of OFMSW and the reduced free water available in the process (García-Bernet et al., 2011; Kayhanian, 1999). For example, HS-AD of OFMSW can be operated at NH_3 content up to 2.7 g N/kg (i.e. 0.19 mol N/kg), whereas NH_3 concentrations ≥ 1.0 g N/kg (i.e. 0.07 mol N/kg) are often reported inhibitory for methanogens (Pastor-Poquet et al., 2019a, b). Thus, the NH_3 build-up in HS-AD may lead to VFA accumulation and eventual reactor failure by acidification (i.e. pH ≤ 6.0). On the other hand, acidification might be also the result of substrate overload due to the imbalance between acidogenic-methanogenic growth and/or the elevated organic content of HS-AD (Pastor-Poquet et al., 2018; Staley et al., 2011). Noteworthy, the release of inorganic carbon (i.e. CO_2/HCO_3^-) by acetoclastic methanogens is one of the main pH buffering agents in AD, potentially counteracting reactor acidification (Steyer et al., 2006). Therefore, the risk of acidification might be also affected by the 'non-ideal' effect on the CO_2 liquid-gas transfer (Patón et al., 2018).

This study evaluates for the first time the main effects of including 'non-ideal' bio-physical-chemical corrections in HS-AD simulations using OFMSW as substrate, at TS contents from 10 to 40 %. With this aim, a relatively simple 'non-ideal' calculation module, based on the Visual MINTEQ (Allison et al., 1991) and Phreeqc (Parkhurst & Appelo, 1999) physical-chemical engines, was developed to assess the potential effects of a high I (e.g. > 0.2 M) upon the main ionic equilibriums of HS-AD, while speeding-

up model simulations. Coupling the proposed 'non-ideal' module with the HS-AD model (Pastor-Poquet et al., 2018) permitted to explore some of the main inhibitory mechanisms (i.e. NH_3 buildup and acidification) in HS-AD of OFMSW, particularly at relatively high TS contents (i.e. ≥ 20 %).

2 METHODOLOGY

2.1 Activity Coefficients and Modified Equilibrium Constants

In this study, the Extended Debye-Hückel (EDH) equation [Equation 8] was used to approximate the activity coefficients (γ_i) in HS-AD. EDH is a particular case of the WATEQ Debye-Hückel equation [Equation 7], whose parameters (A, B and a_i^0) are known for the main ionic species usually measured in AD (e.g. CH_3COO^-, $CH_3CH_2COO^-$, NH_4^+ and Na^+) (Ball & Nordstrom, 1991; Stumm & Morgan, 1996). Importantly, the activity coefficients for non-charged species (γ_0) in solution (i.e. NH_3 and CO_2) were also calculated as a function of *I* [Equation 9], using b_i = 0.1 (Parkhurst & Appelo, 1999).

$$log_{10}(\gamma_i) = -\frac{A \cdot {Z_i}^2 \cdot \sqrt{I}}{1 + B \cdot a_i^0 \cdot \sqrt{I}} \quad (8)$$

$$log_{10}(\gamma_0) = -\, b_i \cdot I \quad (9)$$

To include 'non-ideal' effects in AD, the 'ideal' dissociation/equilibrium constants ($K_{a,i}$) were corrected in terms of activities (a_i) to obtain the modified equilibrium constants ($K_{a,i}$') (Nielsen et al., 2008; Tait et al., 2012). For example, $K_{a,in}$ expressed in activity terms [Equation 10] can be reorganized to obtain the modified equilibrium

158 constant for inorganic nitrogen ($K_{a,in}'$) [Equation 11]. Importantly, the proton activity
159 (a_{h+}) must be used for pH calculations [Equation 12] under 'non-ideal' conditions
160 (Allison et al., 1991; Parkhurst & Appelo, 1999). Therefore, since the 'non-ideal' set of
161 equations (i.e. Equations 2, 8, 9, 11 and 12) is implicit in S_{h+}, the calculation of pH, *I*,
162 and $K_{a,i}'$ must be solved iteratively, fulfilling both equilibriums and mass balances in an
163 ionic solution.
164

$$K_{a,in} = \frac{a_{nh_3} \cdot a_{h^+}}{a_{nh_4^+}} = \frac{\gamma_{nh_3} \cdot S_{nh_3} \cdot \gamma_{h^+} \cdot S_{h^+}}{\gamma_{nh_4^+} \cdot S_{nh_4^+}} = \frac{\gamma_{nh_3} \cdot \gamma_{h^+}}{\gamma_{nh_4^+}} \cdot \frac{S_{nh_3} \cdot S_{h^+}}{S_{nh_4^+}} \quad (10)$$

$$K_{a,in}' = K_{a,in} \cdot \frac{\gamma_{nh4^+}}{\gamma_{nh_3} \cdot \gamma_{h^+}} = \frac{S_{nh_3} \cdot S_{h^+}}{S_{nh_4^+}} \quad (11)$$

$$pH = -log_{10}(a_{h^+}) = -log_{10}(\gamma_{h^+} \cdot S_{h^+}) \quad (12)$$

165
166 For this study, the main global species used were acetate (S_{ac}), propionate (S_{pro}),
167 butyrate (S_{bu}), valerate (S_{va}), inorganic carbon (S_{ic}), inorganic nitrogen (S_{in}), and mono-
168 valent inorganic cations (S_{cat}) and anions (S_{an}), as originally proposed in ADM1
169 (Batstone et al., 2002). The schematic representation of the iterative module for
170 including the 'non-ideality' of an AD solution is shown in Figure 1. All the required
171 equilibrium constants for an 'ideal' solution ($K_{a,i}$) and their temperature dependence
172 using the van't Hoff equation were extracted from Batstone et al. (2002) and Lide
173 (2004).
174
175 To keep the physical-chemical module as simple as possible, the proposed calculation
176 procedure did not consider ion-pairing or precipitation. Noteworthy, ion-pairing and
177 precipitation are based on further ionic equilibriums, whereas the due kinetic rates of

nucleation and crystal growth phenomena must be adequately accounted also for precipitation (Huber et al., 2017; Vaneeckhaute et al., 2018). Further information about those mechanisms and some potential strategies for their implementation in ADM1-based models can be found elsewhere (Flores-Alsina et al., 2015; Lizarralde et al., 2015; Mbamba et al., 2015; Parkhurst & Appelo, 1999; Vaneeckhaute et al., 2018), as also mentioned in section 3.1.3.

The gaseous species used in this study were CH_4, H_2, CO_2, and NH_3. The addition of the NH_3 liquid-gas transfer in the HS-AD model was shown elsewhere (Pastor-Poquet et al., 2018). The Henry's constant ($K_{H,i}$) of each gaseous species was modified by the introduction of γ_0, obtaining the modified Henry's constant ($K_{H,i}'$) [Equation 13]. The $K_{H,i}$ reference values and their dependence with temperature via the van't Hoff equation were extracted from Batstone et al. (2002) and Lide (2004).

$$K_{H,i}{}'\left(\frac{kmol}{m^3 \cdot bar}\right) = \frac{K_{H,i}\left(\frac{kmol}{m^3 \cdot bar}\right)}{\gamma_0} = \frac{S_{g,i}\left(\frac{kmol}{m^3}\right)}{P_i\ (bar)} \quad (13)$$

2.2 Model Implementation Verification

2.2.1 Model Comparison

The 'non-ideal' calculation module [Figure 1] was used to upgrade the CSTR implementation of ADM1 as suggested by Rosén and Jeppsson (2006), and the HS-AD model proposed by Pastor-Poquet et al. (2018). Four different models were compared: standard ADM1 (ADM1); ADM1 using 'non-ideal' conditions (ADM1 Non-Ideal); the HS-AD model (HS-AD Model); and the HS-AD model using 'non-ideal' conditions

(HS-AD Model Non-Ideal). 365 days of continuous HS-AD operation were used in each simulation. Apparent (i.e. kmol/m^3 Solvent) and global (i.e. kmol/m^3 Total) concentrations were used to express exactly the same HS-AD results, since both concentrations are related to each other by the TS, as well as global (ρ_{Global}) and solvent ($\rho_{Solvent}$) specific weights (Pastor-Poquet et al., 2018). Particularly, apparent concentrations were used in the HS-AD model to account for the TS concentration effect on all the soluble species in a low water environment as HS-AD.

Importantly, simulation of a continuous HS-AD reactor using the HS-AD model required the reduction of the volumetric effluent ($Q_{Effluent}$) compared to the influent ($Q_{Influent}$) to maintain V_{Global} constant. With this aim, a proportional controller for $Q_{Effluent}$ was used as described by Pastor-Poquet et al. (2018), allowing also the comparison between the steady-state results obtained with the CSTR implementation of ADM1 and the HS-AD model. On the other hand, all the simulated TS and VS were recalculated (i.e. TS_{Recalc} and VS_{Recalc}, respectively) as shown by Pastor-Poquet et al. (2018), to include the potential losses of volatile materials (i.e. CO_2, NH_3 and VFA) when drying a sample at 105ºC (EPA, 2001). The organic loading rate (OLR) was approximated as the daily influent COD per unit of V_{Global} (i.e. kg COD/$m^3 \cdot$d), while the hydraulic retention time (HRT) was evaluated as the quotient between V_{Global} and $Q_{Effluent}$ (i.e. days). The overall biomass content ($X_{biomass}$) was the sum of all microbial concentrations in ADM1: $X_{biomass} = X_{su} + X_{aa} + X_{fa} + X_{c4} + X_{pro} + X_{ac} + X_{h2}$.

As a novel approach, the four model configurations presented above were used to assess simultaneously the influence of the varying reactor content mass/volume, the effect of

the apparent concentrations, and the solution 'non-ideality' in HS-AD simulations. The biochemical rates used for model verification are reported in Table 1. All the model parameters were as in Rosén and Jeppsson (2006) for mesophilic (35ºC) AD. Continuous influent conditions were used at 10, 20 and 30 % TS [Supplementary Information], together with a $Q_{Influent}$ of 170 m^3/d, a V_{Global} of 3400 m^3, and a reactor design volume ($V_{Reactor}$) of 3700 m^3. With these specifications, all the simulations were performed at an HRT of 20 d, while the OLR was proportionally increased for higher TS influents. All the influent conditions simulated an OFMSW inflow with a relatively high content of proteins (X_{pr}) at different dilutions, permitting to assess differently the NH_3 inhibition on acetate uptake, particularly when reaching steady-state HS-AD.

2.2.2 'Non-Ideal' Calculations

pH calculations were performed as shown in Rosén and Jeppsson (2006) and Volcke et al. (2005). In order to implement 'non-ideal' conditions, the $K_{a,i}$ of all the ionic species in ADM1 (i.e. S_{in}, S_{ic}, S_{ac}) were modified at each time-step, as shown in section 2.1. For 'non-ideal' simulations, S_{cat} and S_{an} were entirely associated to Na^+ and Cl^-, respectively. Importantly, apparent concentrations (i.e. $kmol/m^3$ Solvent) were used in the pH calculations – as well as in all the bio-physical-chemical dynamics – of the HS-AD model, in contrast to the CSTR implementation of ADM1 that used global concentrations (i.e. $kmol/m^3$ Total).

In some HS-AD model simulations, the Phreeqc engine (Charlton & Parkhurst, 2011; Parkhurst & Appelo, 1999) was used for pH, *I* and γ_i calculations, as an alternative to the proposed 'non-ideal' module [Figure 1]. In these cases, precipitation was not used,

249 though ion pairing is one of the main features of Phreeqc. It must be mentioned that the
250 proposed module for assessing 'non-ideality' in HS-AD simulations [Figure 1] is a
251 simplification of more complex physical-chemical engines (i.e. Visual MINTEQ and
252 Phreeqc). Nonetheless, the proposed 'non-ideal' module – instead of Phreeqc – served
253 to compare 'ideal' and 'non-ideal' HS-AD simulations, using the same pH calculation
254 routine in both cases, by only modifying the equilibrium constants ($K_{a,i}$) at each
255 simulation time-step in the 'non-ideal' implementation.
256
257 To illustrate the existing link between 'non-ideality' and the main NH_3 inhibition
258 parameters in structured HS-AD models, the NH_3 half-inhibition constant for
259 acetoclastic methanogens ($K_{i,Snh3,Xac}$) was slightly modified in some cases. Thus,
260 simulations using the original $K_{i,Snh3,Xac}$ for mesophilic (35ºC) conditions (i.e. 0.0018
261 kmol N/m^3) (Batstone et al., 2002) were compared with simulations using slightly
262 different $K_{i,Snh3,Xac}$ (i.e. 0.0008 and 0.0028 kmol N/m^3). To compare the different values
263 for the soluble acetate concentration (S_{ac}) under 'ideal' ($S_{ac,Ideal}$) and 'non-ideal' ($S_{ac,Non-Ideal}$) conditions at the same influent TS, the relative acetate difference was used
264
265 [Equation 14]. To compare the different values for the NH_3 concentration (S_{nh3}) under
266 'ideal' ($S_{nh3,Ideal}$) and 'non-ideal' ($S_{nh3,Non-Ideal}$) conditions, the relative NH_3 difference
267 was used [Equation 15]. The Henry's constant for CO_2 ($K_{H,co2}$) reduction between
268 'ideal' ($K_{H,co2,Ideal}$) and 'non-ideal' ($K_{H,co2,Non-Ideal}$) conditions was also expressed as
269 relative difference [Equation 16].
270

$$Acetate\ Difference\ (\%) = \frac{(S_{ac,Non-Ideal} - S_{ac,Ideal})}{S_{ac,Ideal}} \cdot 100 \qquad (14)$$

$$NH_3\ Difference\ (\%) = \frac{(S_{nh3,Non-Ideal} - S_{nh3,Ideal})}{S_{nh3,Ideal}} \cdot 100 \quad (15)$$

$$K_{H,co2}\ Difference\ (\%) = \frac{(K_{H,co2,Non-Ideal} - K_{H,co2,Ideal})}{K_{H,co2,Ideal}} \cdot 100 \quad (16)$$

271

272

273 **2.3 Experimental Data and Model Calibration**

274 A HS-AD batch experiment fed with OFMSW and using an inoculum-to-substrate ratio
275 (ISR) = 1.0 g VS/g VS at thermophilic (55ºC) conditions was used for model
276 calibration. The batch experiment consisted of a sacrifice test with 15 replicates starting
277 at 15 % TS, where one replicate was opened – 'sacrificed' – periodically, and the main
278 physical-chemical analyses (e.g. TS, VFA) were performed. Experimental data included
279 the cumulative methane production, biogas composition (i.e. CH_4 and CO_2), TS and VS,
280 TAN, VFA, pH, and mono-valent ions (i.e. Na^+, K^+ and Cl^-). The biogas production and
281 composition was the average ± standard deviation of all (remaining) replicates,
282 including that being subsequently emptied. The rest of analyses were performed in
283 triplicate for the punctually-emptied replicate. Manual agitation was only performed
284 while sampling the reactors. Further information about the experimental setup and the
285 physical-chemical analyses used can be found Pastor-Poquet et al. (2019a).

286

287 For calibration, the 'non-ideal' CSTR implementation of ADM1 (ADM1 Non-Ideal)
288 and the HS-AD model (HS-AD Model Non-Ideal) were compared, using the
289 biochemical rates reported in Table 1. Noteworthy, these rates were slightly different
290 than those used in the original ADM1 implementation (Batstone et al., 2002), since a
291 new population for valerate degraders (X_{c5}) was included, while the composite (X_c)
292 disintegration was disregarded, as shown by Pastor-Poquet et al. (2018). As an example,

293 a reversible (non-competitive) NH_3 inhibition function [Equation 17] was also used for
294 propionate and valerate uptakes in model calibration [Table 1], to account for the
295 potential methanogenic and/or acetogenic NH_3 inhibition observed in the experimental
296 dataset (Pastor-Poquet et al., 2018). The initial conditions were recalculated based on
297 the experimental data available. The biochemical parameters for thermophilic (55ºC)
298 conditions were extracted from Batstone et al. (2002). Meanwhile, some parameters
299 were also modified aiming to fit adequately the experimental data [Table 2]. Parameter
300 calibration and all the initial biomass concentrations (e.g. X_{ac}) were approximated by
301 trial-and-error. The detailed methodology used for obtaining the initial conditions and
302 for model calibration were described elsewhere (Pastor-Poquet et al., 2018).
303

$$I_{nh3} = \frac{K_{i,Snh3}}{K_{i,Snh3} + S_{nh3,App}} \quad (17)$$

304
305 It must be stated that both the initial conditions and/or the biochemical model
306 parameterization are tightly related to the model structure (Dochain & Vanrolleghem,
307 2001; Donoso-Bravo et al., 2011; Poggio et al., 2016). Thus, in order to minimize the
308 differences between the CSTR implementation of ADM1 and the HS-AD model, the
309 same set of initial conditions [Supplementary Information] and thermophilic (55ºC)
310 parameters [Table 2] were used in both cases. The adjustment/fitting of the model
311 implementations regarding the experimental data was evaluated by the weighted sum of
312 squares, calculated as shown by Flotats et al. (2003). The weighted sum of squares
313 included the cumulative methane production (V_{ch4} Cum.), gas composition (CH_4 +
314 CO_2), pH, TAN (S_{in}), and VFA (S_{ac}, S_{pro}, S_{bu} & S_{va}).
315

316

317 **3 RESULTS AND DISCUSSION**

318 **3.1 Verification of the 'Non-Ideal' Model Implementation**

319 **3.1.1 Effects of 'Non-Ideality' on Standard ADM1**

320 The main difference between the 'ideal' ADM1 simulations using different influent TS
321 was the S_{in} and S_{ac} accumulation, but also the reduction of the acetoclastic methanogens
322 concentration (X_{ac}) along higher operating TS [Table 3]. These results are related to the
323 higher OLR used at higher influent TS, since the protein content (i.e. 0.22 kg COD/kg
324 COD), as well as the anaerobic biodegradability (i.e. 0.35 kg COD/kg COD) were set
325 equal for all the influent conditions. Meanwhile, the S_{ac} accumulation at higher influent
326 TS [Figure 2a] was also related to the NH_3 half-inhibition constant for acetoclastic
327 methanogens used in all simulations (i.e. $K_{i,Snh3,Xac}$ = 0.0018 kmol N/m^3), since an
328 increasing S_{nh3} exacerbates inhibition [Table 1]. Thus, the $X_{ac}/X_{biomass}$ ratio was
329 observed to decrease from 20.6 to 16.6 % at 10 and 30 % influent TS, respectively
330 [Figure 2b]. Importantly, this last phenomenon might imply a greater risk of
331 methanogenic overloading at increasing OLR in HS-AD simulations under 'ideal'
332 conditions, since a proportionally lower X_{ac} is available to counteract the S_{ac} buildup.

333

334 The CSTR implementation of ADM1 using 'non-ideal' conditions (ADM1 Non-Ideal)
335 showed an increasing *I* alongside the higher influent TS used, from 0.166 M at 10 % TS
336 up to 0.390 M at 30 % TS [Table 3]. These results suggest that the bio-physical-
337 chemistry in HS-AD of OFMSW might be considerably 'non-ideal' (i.e. $I \geq 0.2$ M),
338 being the solution 'non-ideality' exacerbated at higher operating TS contents and/or by
339 the occurrence of inhibitory mechanisms (i.e. NH_3 build-up). Therefore, an adequate

340 'non-ideal' methodology seems to be required to account for ionic speciation in HS-AD
341 simulations (Batstone et al., 2015; Tait et al., 2012), though the *I* range for HS-AD of
342 OFMSW should be better assessed by experimental data, as shown in section 3.3.
343
344 The 'non-ideal' ADM1 implementation affected practically all the simulated dynamics
345 (e.g. S_{ic}, S_{ac} and X_{ac}), in comparison to the 'ideal' ADM1 implementation [Table 3].
346 Particularly, S_{nh3} decreased by 3 - 45 % when using the 'non-ideal' in contrast to the
347 'ideal' methodology at each operating TS (i.e. 10 - 30 %), substantially mitigating the
348 acetoclastic inhibition and S_{ac} accumulation [Figure 2a]. The potential alleviation of
349 NH_3 inhibition by using 'non-ideal' conditions was also suggested by Hafner and
350 Bisogni (2009) for AD digesters using cow/swine manure as substrate. In this study, the
351 implementation of 'non-ideal' ADM1 calculations also showed an 8 to 20 % increase in
352 the $X_{ac}/X_{biomass}$ ratio at higher TS (i.e. 20 - 30 %) compared to the 'ideal'
353 implementation [Figure 2b]. Thus, 'non-ideal' conditions potentially allow a higher
354 operating OLR when simulating HS-AD of OFMSW, since the reduced S_{nh3} leads to a
355 relatively higher X_{ac} to counteract substrate overloading and S_{ac} accumulation.
356
357 It must be noted that, due to the inherent structure of both the biochemical (i.e. Monod
358 equation) and physical-chemical (i.e. charge balance) framework in ADM1, AD
359 simulations are highly non-linear (Donoso-Bravo et al., 2011; Solon, 2016; Volcke et
360 al., 2005). In other words, an increase in the influent conditions (i.e. OLR) of an
361 ADM1-based model might not lead to a proportional increase in the output dynamics
362 (e.g. S_{ac} and S_{nh3}) at steady-state. For example, the S_{ac} accumulation was observed to
363 increase exponentially alongside the S_{nh3} build-up both with the 'ideal' and 'non-ideal'

implementations of ADM1 [Figure 2c]. This last effect is related to the Monod kinetics, as well as the reversible inhibition function used for acetoclastic methanogenesis in ADM1 [Table 1]. Therefore, the implementation of 'non-ideal' conditions may be crucial in HS-AD simulations, since minimal changes in S_{nh3} – associated to the 'non-ideal' physical-chemistry – might lead to considerable differences in the anaerobic kinetic rates and/or inhibition potential using structured HS-AD models.

Finally, $K_{H,i}$ for gaseous species (i.e. CH_4 and CO_2) decreased linearly alongside increasing *I* by using 'non-ideal' conditions in HS-AD. For example, $K_{H,co2}$ showed a 8.6 % reduction at an *I* of 0.39 M using ADM1 Non-Ideal [Equation 16], corresponding to a 30 % influent TS [Table 3 and Figure 2d]. Similarly, a linear relationship was also obtained for the $K_{H,co2}$ reduction at increasing TS contents from 10 to 40 %: $K_{H,co2}$ *Difference (%) = - 0.242 · TS (%) - 1.343,* r^2 *= 1.000* – data not shown. The $K_{H,i}$ reduction with increasing TS strongly influences the liquid-gas transfer in HS-AD simulations. For example, the $K_{H,co2}$ reduction exacerbates the CO_2 volatilization in HS-AD, potentially reducing the available inorganic carbon content ($S_{ic,}$ HCO_3^-), as an important source of buffering capacity and resistance against organic overloading (Patón et al., 2018; Poggio et al., 2016; Steyer et al., 2006). Therefore, 'non-ideal' conditions are also needed to evaluate the liquid-gas transfer (i.e. CO_2) in HS-AD simulations, as a potential trigger for reactor acidification.

3.1.2. 'Non-Ideal' Implementation of the HS-AD Model

The main difference between the CSTR implementation of ADM1 and the HS-AD model lies on the simulation of M_{Global}, V_{Global}, TS, VS, and ρ_{Global} dynamics by the HS-

AD model (Pastor-Poquet et al., 2018). Moreover, $Q_{Effluent}$ had to be reduced compared to $Q_{Influent}$ when using the HS-AD model, as mentioned in section 2.2.1. Therefore, all simulations using the HS-AD model resulted in noticeable differences in the values of these operational variables (i.e. TS, VS and $Q_{Effluent}$) at steady-state [Table 3], in comparison to the corresponding influent conditions. On the other hand, the use of apparent concentrations (i.e. $S_{ac,App}$, kg COD/m^3 Solvent) increased relatively the soluble global species concentrations (i.e. S_{ac}, kg COD/m^3 Total) at higher operating TS [Table 3], due to the lower amount of free water in HS-AD (Pastor-Poquet et al., 2018).

The previous conclusions about the NH_3 inhibition alleviation and the increasing liquid-gas transfer (i.e. CO_2) using ADM1 Non-Ideal – section 3.1.1 – are also valid for HS-AD Model Non-Ideal. In particular, S_{ac} was from 48 to 93 % lower for 'non-ideal' than 'ideal' HS-AD model simulations [Table 3 and Figure 2a]. However, it must be highlighted that 'non-ideal' conditions were further exacerbated using the HS-AD model, likely due to the inclusion of apparent concentrations in the bio-physical-chemical framework. Thus, HS-AD Model Non-Ideal showed a 5 - 32 % increase on *I* compared to ADM1 Non-Ideal [Table 3]. Meanwhile, the $K_{H,co2}$ reduction [Equation 16] at influent TS contents from 10 to 40 % showed a more pronounced slope than that obtained with ADM1: $K_{H,co2}$ *Difference (%) = - 0.400 · TS (%) + 0.565,* r^2 *= 0.991* – data not shown.

Interestingly, when using HS-AD Model Non-Ideal, some seemingly contradictory results were observed regarding the NH_3 inhibition between the 'ideal' and 'non-ideal' simulations at steady-state: At 30 % influent TS, the apparent NH_3 concentration

($S_{nh3,App}$) was 0.00867 and 0.00868 kmol N/m^3 Solvent (i.e. 0.12 % difference), while S_{ac} was 19.5 and 10.0 kg COD/m^3 Total, for the 'ideal' and 'non-ideal' HS-AD model implementations, respectively [Table 3]. In other words, the steady-state S_{ac} was substantially lower at an equivalent $S_{nh3,App}$. Meanwhile, the steady-state S_{ac} *vs.* S_{nh3} still fulfilled the Monod inhibition framework [Figure 2c].

To emphasize these last results, the relative differences in the acetate [Equation 14] and NH_3 [Equation 15] concentrations were used. Thus, $S_{ac,Non-Ideal}$ was lower than $S_{ac,Ideal}$ – the acetate difference was negative – at any influent TS [Table 3 and Figure 3a]. Nevertheless, the NH_3 difference between $S_{nh3,Non-Ideal}$ and $S_{nh3,Ideal}$ at 30 % TS was positive, in contrast to 10 and 20 % TS influent conditions [Table 3 and Figure 3b]. Similar 'contradictory' results were also observed at higher influent TS contents (i.e. 35 - 40 % TS), where S_{ac} was lower (i.e. 26 - 35 %), while S_{nh3} was higher (i.e. 1 - 3 %), for the 'non-ideal' in contrast to the 'ideal' HS-AD model implementation [Figure 3].

Summarizing, results above seemed to contradict the expected trend for acetoclastic inhibition in HS-AD simulations at steady-state: a higher S_{nh3} concentration should lead to a higher S_{ac} accumulation. However, these seemingly contradictory results on NH_3 inhibition were only related to the direct comparison of two strongly non-linear model implementations (i.e. 'ideal' *vs.* 'non-ideal'). More in particular, during the initial 40 days of HS-AD model simulations using a 30 % influent TS, the X_{ac} growth was promoted by the 'non-ideal' in contrast to the 'ideal' model implementation, due to a lower operating $S_{nh3,App}$, as further discussed in section 3.1.3.

All the above simulations were performed using $K_{i,Snh3,Xac}$ = 0.0018 kmol N/m^3. Importantly, when shifting $K_{i,Snh3,Xac}$ towards lower/higher values in HS-AD Model Non-Ideal, the TS threshold where $S_{ac,Ideal} > S_{ac,Non-Ideal}$ for $S_{nh3,Ideal} < S_{nh3,Non-Ideal}$ ('inversion' threshold) also shifted [Figure 3]. For example, using $K_{i,Snh3,Xac}$ = 0.0008 kmol N/m^3, the 'inversion' threshold occurred at around 20 % influent TS, while using $K_{i,Snh3,Xac}$ = 0.0028 kmol N/m^3, the 'inversion' threshold occurred between 35 and 40 % TS. Similar acetoclastic inhibition results were also obtained between the 'ideal' and 'non-ideal' ADM1 implementations, though the 'inversion' thresholds shifted towards slightly higher operating TS regarding the HS-AD model [Figure 3]. For example, using $K_{i,Snh3,Xac}$ = 0.0018 kmol N/m^3, the 'inversion' threshold using ADM1 was 40 % influent TS, instead of 30 % influent TS. All these results indicate that 'non-ideality' is tightly related to the NH_3 inhibition parameters, but also to the overall HS-AD model structure.

3.1.3 The Effects of 'Non-Ideality' during the Initial Days of HS-AD Simulations

During the initial 20 days of HS-AD simulations using 30 % influent TS, X_{ac} was observed to increase considerably faster under 'non-ideal' than 'ideal' conditions [Figure 4a], explaining the lower S_{ac} buildup under 'non-ideal' conditions [Figure 4b]. pH was equivalent during the initial 10 days of 'ideal' and 'non-ideal' simulations, though pH for 'non-ideal' simulations was up to 0.27 units higher from day 10 [Figure 4c and Table 3]. Meanwhile, a lower $S_{nh3,App}$ was observed along the initial 40 days of 'non-ideal' simulations [Figure 4d], despite the apparent TAN ($S_{in,App}$) was equivalent in both the 'ideal' and 'non-ideal' model implementations [Figure 4e]. Therefore, the 'non-ideal' bio-physical-chemistry of HS-AD at 30 % influent TS led to a lower $S_{nh3,App}$, mitigating the NH_3 inhibition and promoting the X_{ac} growth, as previously

460 observed for 10 and 20 % influent TS. Nonetheless, the steady-state results [Table 3]
461 prevented observing the overall effect of 'non-ideality' in HS-AD simulations.
462
463 With all the above, the 'inversion' threshold on the NH_3 concentration at steady-state
464 [Figure 3b] is the consequence of comparing two strongly non-linear model
465 implementations (i.e. 'ideal' *vs.* 'non-ideal') at steady-state, being non-linearity
466 associated to the complexity of the biochemical and physical-chemical framework of
467 ADM1-based models, as mentioned before. Importantly, the occurrence of the NH_3
468 'inversion' threshold further stresses the fact that 'ideal' ADM1-based models should
469 not be applied to HS-AD (i.e. TS $\geq$ 10 %), since the equation non-linearities might lead
470 to important differences in both the dynamics and the steady state results (i.e. pH, X_{ac},
471 S_{nh3}, S_{ac}) of HS-AD simulations. The 'inversion' threshold on the NH_3 inhibition at
472 steady-state was also observed when using slightly different initial conditions (i.e. $X_{pr,0}$,
473 $S_{in,0}$, $S_{ac,0}$, $S_{cat,0}$, $X_{su,0}$ and/or $X_{aa,0}$ – data not shown), since steady-state AD simulations
474 should not depend on the initial conditions used (Donoso-Bravo et al., 2011). Thus, all
475 the above results indicate that a high *I* (i.e. $\geq$ 0.2 M) strongly influenced the bio-
476 physical-chemistry of HS-AD simulations, particularly the NH_3 inhibition dynamics
477 during the initial days of reactor operation at high TS contents (i.e. $\geq$ 20 - 30 %).
478
479 To assess 'non-ideal' effects on AD, some of the most complete physical-chemical
480 engines for 'non-ideal' characterizations are Visual MINTEQ (Allison et al., 1991) and
481 Phreeqc (Parkhurst & Appelo, 1999) software, including the direct ADM1
482 implementation in Phreeqc (C code) described by Huber et al. (2017), the generic
483 nutrient recovery model of Vaneeckhaute et al. (2018), but also the physical-chemical

484 module developed by Flores-Alsina et al. (2015) and Solon et al. (2015) for plant-wide
485 wastewater treatment. Indeed, the high organic content in HS-AD might strongly
486 determine the precipitation, ion-pairing and ion-surface interactions (Batstone et al.,
487 2012; Huber et al., 2017), requiring even further complexity of the HS-AD bio-
488 physical-chemical framework than for 'wet' AD applications (i.e. TS < 10 %). On the
489 other hand, more simple 'non-ideal' modules for AD solutions have been also used by
490 Patón et al. (2018) and Nielsen et al. (2008). In this line, the model complexity depends
491 on the model objectives and experimental data available, being always recommended to
492 keep the model as simple as possible, though well suited for addressing the envisaged
493 objectives (Eberl et al., 2006).
494
495 To validate the 'non-ideal' module proposed in this study [Figure 1], 'non-ideal'
496 simulations of the HS-AD model were also performed coupling the Phreeqc engine
497 (Charlton & Parkhurst, 2011). In spite of the higher complexity of Phreeqc, both 'non-
498 ideal' modules yielded practically the same HS-AD dynamics (i.e. S_{ac}, S_{in}, X_{ac}) using 30
499 % influent TS [Figure 3], being the 2 - 6 % higher *I* the most noticeable difference when
500 Phreeqc was used as 'non-ideal' module [Figure 3f]. The Phreeqc engine coupling to
501 the HS-AD model also yielded closely-matching results to the proposed 'non-ideal'
502 module under all the HS-AD simulations presented in section 3.1.2 – data not shown.
503 Importantly, due to the reduced complexity of the proposed 'non-ideal' module [Figure
504 1] and/or the coupling of an 'external' software, the simulation speed increased
505 considerably (i.e. 7 - 8 times faster) compared to when using the Phreeqc engine as
506 'non-ideal' module.
507

508 **3.2 HS-AD Calibration under 'Non-Ideal' Conditions**

509 The calibration in this study was not aimed to be exhaustive due to the great number of
510 parameters (i.e. > 15) and initial conditions (i.e. > 10) involved in an ADM1-based
511 model, as well as the reduced number of experimental data available (Dochain &
512 Vanrolleghem, 2001; Donoso-Bravo et al., 2011; Poggio et al., 2016). Instead, the
513 calibration aimed to assess the operative levels of *I* in HS-AD of OFMSW. Moreover,
514 real data calibration could also serve to evaluate the influence of the model complexity
515 (i.e. mass balances) regarding the need for 'non-ideal' calculations in HS-AD.
516
517 For the calibration of ADM1 Non-Ideal and HS-AD Model Non-Ideal, the same initial
518 conditions and biochemical parameters [Table 2] were used, yielding a similar degree of
519 adjustment regarding the experimental data (i.e. weighted sum of squares = 2.2 - 2.5)
520 [Supplementary Information]. Nonetheless, HS-AD Model Non-Ideal outperformed
521 ADM1 Non-Ideal in terms of simulating the TS, VS, and M_{Global} dynamics due to the
522 use of a more extended set of mass balances. Moreover, HS-AD Model Non-Ideal
523 adjustment improved considerably towards the end of the experiment, in contrast to the
524 ADM1 Non-Ideal simulations [Figure 5]. For example, the experimental matching in
525 S_{in}, S_{pro}, S_{va}, and gas composition improved from day 15 - 20 onwards, as M_{Global} and/or
526 V_{Global} reduction by methanogenesis occurred in the system. In this line, HS-AD Model
527 Non-Ideal predicted 1.6 g of M_{Global} were removed, equivalent to a 4.4 % of the initial
528 reactor content, during 92 days of batch operation.
529
530 Both ADM1 Non-Ideal and HS-AD Model Non-Ideal simulations showed $I \geq 0.5$ M
531 from day 50 [Figure 5d], associated to the accumulation of S_{in} and VFA, with *I* being

around 5 - 10 % higher in HS-AD Model, due to the use of apparent concentrations. These results confirm that *I* might be considerably higher than 0.2 M in HS-AD of OFMSW, strongly suggesting the implementation of 'non-ideal' conditions at high TS contents (i.e. ≥ 10 %) to improve the simulations of pH, biochemical inhibition (i.e. NH_3), VFA accumulation (i.e. acetate), and liquid-gas transfer (i.e. CO_2). Furthermore, taking into account the high *I* observed (i.e. ≥ 0.5 M), the Davies equation [Equation 6] might not be appropriated for HS-AD simulations due to the increasing errors in γ_i at $I \geq$ 0.2 M. For example, a 20 to 25 % higher γ_{NH4+} is obtained at *I* of 0.5 and 0.6 M, respectively, by using the Davies instead of the EDH equation [Equation 8].

With all the above, the influence of 'non-ideality' on the bio-physical-chemistry of HS-AD simulations strongly depends on the model configuration used. Therefore, the HS-AD model (Pastor-Poquet et al., 2018) may be well suited to assess 'non-ideal' effects in HS-AD using OFMSW as a substrate, and particularly the TS concentration effect on the soluble species by using apparent concentrations. Noteworthy, the implementation of apparent concentrations (i.e. kmol/kg Solvent) is in line with the fact that the bio-physical-chemistry of HS-AD occurs predominantly in water. Thus, using apparent concentrations might enhance the predictive capabilities of the 'non-ideal' calculation procedure, while influencing both the kinetic rates and inhibition of anaerobic microorganisms in HS-AD simulations (Pastor-Poquet et al., 2018). On the other hand, an adequate mass balance implementation in HS-AD models is needed when using relatively long simulations (i.e. ≥ 20 days), as the effect of reactor mass/volume removal by methanogenesis becomes gradually more important to capture all the bio-physical-chemical mechanisms in HS-AD.

To end up, further calibration/optimization alongside a thorough sensitivity analysis is needed for the main biochemical parameters of the HS-AD model, in order to draw adequate conclusions about some of the inhibitory mechanisms (i.e. NH_3 buildup and acidification) potentially occurring in HS-AD of OFMSW. In this line, the faster HS-AD model resolution obtained when coupling the proposed 'non-ideal' module might be particularly suited to speed up the calibration process, where a great number of simulations are usually required to match appropriately the experimental data (Dochain & Vanrolleghem, 2001; Donoso-Bravo et al., 2011; Flotats et al., 2006). Alongside, further bio-physical-chemical mechanisms as precipitation, ion pairing and ion-surface interactions should be also evaluated in future model implementations, to adequately address the inherent complexity of HS-AD using OFMSW as substrate.

4 CONCLUSIONS

HS-AD of OFMSW might be operated at $I \geq 0.5$ M. Therefore, the bio-physical-chemistry of all HS-AD simulations needs to account for the 'non-ideal' effects on the pH, soluble inhibitors (i.e. NH_3), and liquid-gas transfer (i.e. CO_2), particularly at higher TS contents (i.e. ≥ 20 %). In this study, coupling a HS-AD model to a simplified 'non-ideal' module yielded adequate simulations regarding the NH_3 inhibition in HS-AD, both in batch and continuous mode. Using an appropriate set of parameters, the HS-AD model using 'non-ideal' conditions might bring further insights about the main inhibitory mechanisms in HS-AD of OFMSW.

Acknowledgements
This project has received funding from the European Union's Horizon 2020 research and innovation programme under the Marie Sklodowska-Curie grant agreement No. 643071.

REFERENCES

Allison, J.D., Brown, D.S., Novo-Gradac, K.J. 1991. MINTEQA2/PRODEFA2, a geochemical assessment model for environmental systems: Version 3.0 users's manual. U.S. Environmental Protection Agency (EPA).

Ball, J.W., Nordstrom, D.K. 1991. User's manual for WATEQ4F, with revised thremodynamic data base and test cases for calculating speciation of major, trace and redox elements in natural waters. U.S. Geological Survey.

Batstone, D.J., Amerlinck, Y., Ekama, G., Goel, R., Grau, P., Johnson, B., . . . Volcke, E. 2012. Towards a generalized physicochemical framework. *Water Sci. Technol.*, **66**(6), 1147-1161.

Batstone, D.J., Keller, J., Angelidaki, I., Kalyuzhnyi, S.V., Pavlostathis, S.G., Rozzi, A., . . . Vavilin, V.A. 2002. The IWA Anaerobic Digestion Model No. 1 (ADM1). *Water Sci. Technol.*, **45**(10), 65-73.

Batstone, D.J., Puyol, D., Flores-Alsina, X., Rodríguez, J. 2015. Mathematical modelling of anaerobic digestion processes: Applications and future needs. *Rev. Environ. Sci. Bio.*, **14**(4), 595-613.

Charlton, S.R., Parkhurst, D.L. 2011. Modules based on the geochemical model PHREEQC for use in scripting and programming languages. *Comput. Geosci.*, **37**(10), 1653-1663.

Dochain, D., Vanrolleghem, P. 2001. *Dynamical Modelling and Estimation in Wastewater Treatment Processes*. IWA Publishing, London, UK.

Donoso-Bravo, A., Mailier, J., Martin, C., Rodríguez, J., Aceves-Lara, C.A., Vande Wouwer, A. 2011. Model selection, identification and validation in anaerobic digestion: A review. *Water Res.*, **45**(17), 5347-5364.

Eberl, H.J., Morgenroth, E., Noguera, D.R., Picioreanu, C., Rittmann, B.E., van Loosdrecht, M.C., Wanner, O. 2006. *Mathematical Modeling of Biofilms*. IWA Publishing, London, UK.

EPA. 2001. Method 1684. Total, fixed and volatile solids in water, solids, and biosolids. U.S. Environmental Protection Agency (EPA).

Flores-Alsina, X., Kazadi Mbamba, C., Solon, K., Vrecko, D., Tait, S., Batstone, D.J., . . . Gernaey, K.V. 2015. A plant-wide aqueous phase chemistry module describing pH variations and ion speciation/pairing in wastewater treatment process models. *Water Res.*, **85**, 255-265.

Flotats, X., Ahring, B.K., Angelidaki, I. 2003. Parameter identification of thermophilic anaerobic degradation of valerate. *Appl. Biochem. Biotechnol.*, **109**(1-3), 47-62.

Flotats, X., Palatsi, J., Ahring, B.K., Angelidaki, I. 2006. Identifiability study of the proteins degradation model, based on ADM1, using simultaneous batch experiments. *Water Sci. Technol.*, **54**(4), 31-39.

García-Bernet, D., Buffière, P., Latrille, E., Steyer, J.-P., Escudié, R. 2011. Water distribution in biowastes and digestates of dry anaerobic digestion technology. *Chem. Eng. J.*, **172**(2-3), 924-928.

Hafner, S.D., Bisogni, J.J. 2009. Modeling of ammonia speciation in anaerobic digesters. *Water Res.*, **43**(17), 4105-4114.

Huber, P., Neyret, C., Fourest, E. 2017. Implementation of the anaerobic digestion model (ADM1) in the PHREEQC chemistry engine. *Water Sci. Technol.*, **76**(5-6), 1090-1103.

Kayhanian, M. 1999. Ammonia inhibition in high-solids biogasification: an overview and practical solutions. *Environ. Technol.*, **20**(4), 355-365.

Kayhanian, M., Tchobanoglous, G. 1996. Development of a mathematical model for the simulation of the biodegradation of organic substrates in a high-solids anaerobic digestion. *J. Chem. Tech. Biotechnol.*, **66**, 312-322.

Lauwers, J., Appels, L., Thompson, I.P., Degrève, J., Van Impe, J.F., Dewil, R. 2013. Mathematical modelling of anaerobic digestion of biomass and waste: Power and limitations. *Prog. Energy Combust. Sci.*, **39**, 383-402.

Lide, D.R. 2004. *Hanbook of chemistry and physics*. *84th ed*. CRC Press.

Lizarralde, I., Fernández-Arévalo, T., Brouckaert, C., Vanrolleghem, P., Ikumi, D.S., Ekama, G.A., . . . Grau, P. 2015. A new general methodology for incorporating physico-chemical transformations into multi-phase wastewater treatment process models. *Water Res.*, **74**, 239-256.

Mbamba, C.K., Tait, S., Flores-Alsina, X., Batstone, D.J. 2015. A systematic study of multiple minerals precipitation modelling in wastewater treatment. *Water Res.*, **85**, 359-370.

Nielsen, A.M., Spanjers, H., Volcke, E.I. 2008. Calculating pH in pig manure taking into account ionic strength. *Water Sci. Technol.*, **57**(11), 1785-90.

Parkhurst, D.L., Appelo, C.A.J. 1999. User's guide to PHREEQC (version 2) - A computed program for speciation, batch-reaction, one-dimentional transport and inverse geochemical calculations. U.S. Geological Survey.

Pastor-Poquet, V., Papirio, S., Steyer, J.-P., Trably, E., Escudié, R., Esposito, G. 2018. High-solids anaerobic digestion model for homogenized reactors. *Water Res.*, **142**, 501-511.

Pastor-Poquet, V., Papirio, S., Trably, E., Rintala, J., Escudié, R., Esposito, G. 2019a. High-Solids Anaerobic Digestion requires a tradeoff between Total Solids, Inoculum-to-Substrate Ratio and Ammonia Inhibition. *Int. J. Environ. Sci. Technol.*.

Pastor-Poquet, V., Papirio, S., Trably, E., Rintala, J., Escudié, R., Esposito, G. 2019b. Semi-continuous Mono-digestion of OFMSW and Co-digestion of OFMSW with Beech Sawdust: Assessment of the Maximum Operational Total Solid Content. *J. Environ. Manage.*, **231**, 1293-1302.

Patón, M., González-Cabaleiro, R., Rodríguez, J. 2018. Activity corrections are required for accurate anaerobic digestion modelling. *Water Sci. Technol.*, **77**(7-8), 2057-2067.

Poggio, D., Walker, M., Nimmo, W., Ma, L., Pourkashanian, M. 2016. Modelling the anaerobic digestion of solid organic waste - Substrate characterisation method for ADM1 using a combined biochemical and kinetic parameter estimation approach. *Waste Manage.*, **53**, 40-54.

Rosén, C., Jeppsson, U. 2006. Aspects on ADM1 implementation within the BSM2 framework. Division of Industrial Electrical Engineering and Automation, Faculty of Engineering, Lund University, Sweden.

Solon, K. 2016. Physico-Chemical Modelling (PCM) - A literature review. Division of Industrial Electrical Engineering and Automation, Faculty of Engineering, Lund University, Sweden.

Solon, K., Flores-Alsina, X., Mbamba, C.K., Volcke, E.I., Tait, S., Batstone, D., . . . Jeppsson, U. 2015. Effects of ionic strength and ion pairing on (plant-wide) modelling of anaerobic digestion. *Water Res.*, **70**, 235-245.

Staley, B.F., de Los Reyes III, F.L., Barlaz, M.A. 2011. Effect of spatial differences in microbial activity, pH, and substrate levels on methanogenesis initiation in refuse. *Appl. Environ. Microbiol.*, **77**(7), 2381-2391.

Steyer, J.P., Bernard, O., Batstone, D.J., Angelidaki, I. 2006. Lessons learnt from 15 years of ICA in anaerobic digesters. *Water Sci. Technol.*, **53**(4-5), 25-33.

Stumm, W., Morgan, J.J. 1996. *Aquatic Chemistry. Chemical Equilibria and Rates in Natural Waters. 3rd ed*. John Wiley & Sons, USA.

Tait, S., Solon, K., Volcke, E., Batstone, D. 2012. A unified approach to modelling wastewater chemistry model corrections. *3rd Wastewater Treatment Modelling Seminar (WWTmod2012)*, Mont-Sainte-Anne, Quebec, Canada. International Water Association.

Vaneeckhaute, C., Claeys, F.H.A., Tack, F.M.G., Meers, E., Belia, E., Vanrolleghem, P.A. 2018. Development, implementation, and validation of a generic nutrient recovery model (NRM) library. *Environ. Model. Software*, **99**, 170-209.

Volcke, E., Van Hulle, S., Deksissa, T., Zaher, U., Vanrolleghem, P. 2005. Calculation of pH and concentration of equilibrium components during dynamic simulation by means of a charge balance. Universiteit Gent, Belgium.

Xu, F., Li, Y., Wang, Z.-W. 2015. Mathematical modeling of solid-state anaerobic digestion. *Prog. Energy Combust. Sci.*, **51**, 49-66.

TABLE CAPTIONS

Table 1: Biochemical rates used for model implementation verification and model calibration.

Table 2: Biochemical parameters modified for model calibration at thermophilic (55ºC) conditions.

Table 3: Summary of steady-state results (i.e. day 365) for model implementation verification at different influent total solid (TS) contents.

FIGURE CAPTIONS

Figure 1: Schematic representation of the 'ideal' or 'non-ideal' physical-chemical implementation used for all ADM1-based models in this study.

Figure 2: Summary of results for model implementation verification as a function of influent total solids (TS). Comparison between standard ADM1, ADM1 Non-Ideal, HS-AD Model and HS-AD Model Non-Ideal outputs: a) Total acetate concentration (S_{ac}) *vs.* initial TS; b) total acetoclastic methanogens to biomass ratio ($X_{ac}/X_{biomass}$) *vs.* initial TS; c) total acetate concentration (S_{ac}) *vs.* total NH_3 concentration (S_{nh3}); and d) Henry's constant difference for CO_2 ($K_{H,co2}$) *vs.* ionic strength.

Figure 3: Contour plots for the relative difference between the 'ideal' and 'non-ideal' implementations of both ADM1 and the HS-AD model at different influent total solid (TS) contents: a) Acetate (S_{ac}) difference [Equation 14]; and b) NH_3 (S_{nh3}) difference [Equation 15].

Figure 4: Effect of 'non-ideality' during the initial 40 days of HS-AD model simulations at 30 % influent TS. Comparison between 'ideal' and 'non-ideal' conditions, including the Phreeqc engine: a) Acetoclastic methanogens concentration (X_{ac}); b) total acetate concentration (S_{ac}); c) pH; d) apparent NH_3 concentration ($S_{nh3,App}$); e) total ammonia nitrogen concentration ($S_{in,App}$); and f) ionic strength (I).

Figure 5: Model calibration results. Comparison between ADM1 Non-Ideal and HS-AD Model Non-Ideal: a) Total ammonia nitrogen (TAN); b) total propionate (S_{pro}) and valerate (S_{va}) concentrations; c) gas composition; and d) ionic strength.

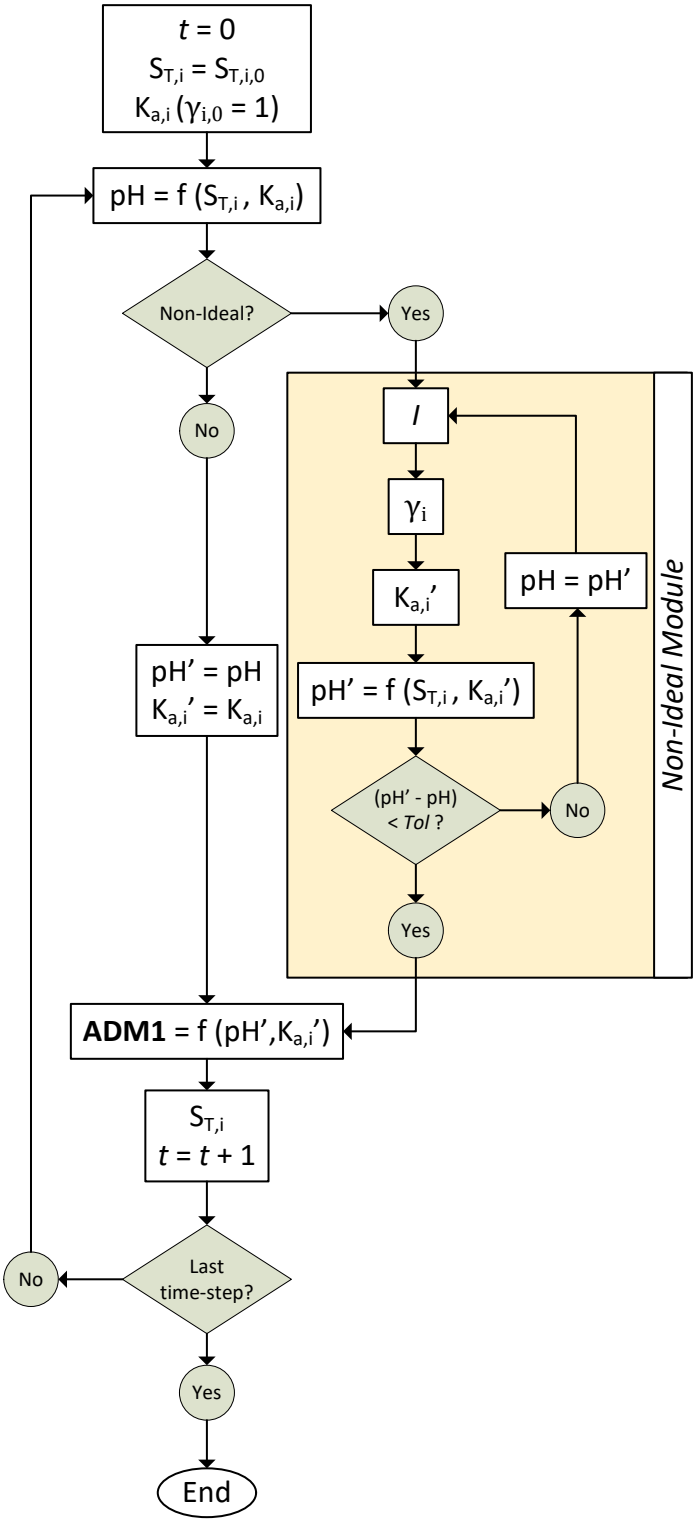

Figure 1: Schematic representation of the 'ideal' or 'non-ideal' physical-chemical implementation used for all ADM1-based models in this study.

NOTE: *t* refers to the simulation time-step. *Tol* refers to tolerance (in this study $Tol = 10^{-6}$). *I* is the ionic strength; while $S_{T,i}$ is the global concentration; $K_{a,i}$ is the dissociation equilibrium constant; and γ_i is the activity coefficient of soluble species.

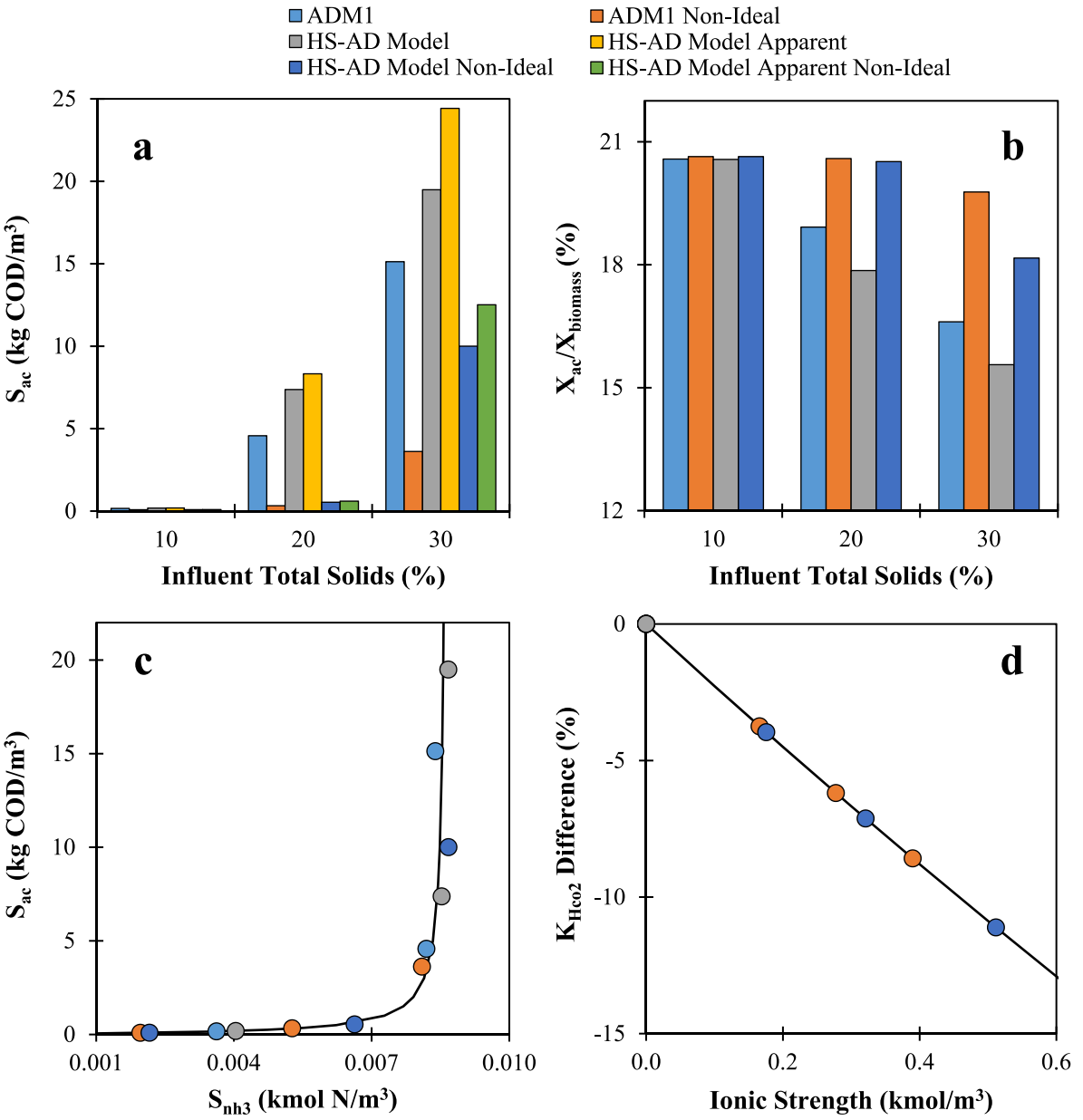

Figure 2: Summary of results for model implementation verification as a function of influent total solids (TS). Comparison between standard ADM1, ADM1 Non-Ideal, HS-AD Model and HS-AD Model Non-Ideal outputs: a) Total acetate concentration (S_{ac}) vs. initial TS; b) total acetoclastic methanogens to biomass ratio ($X_{ac}/X_{biomass}$) vs. initial TS; c) total acetate concentration (S_{ac}) vs. total NH_3 concentration (S_{nh3}); and d) Henry's constant difference for CO_2 ($K_{H,co2}$) vs. ionic strength.

NOTE: The global (i.e. kg COD/m^3 Total) and apparent (i.e. kg COD/m^3 Solvent) concentrations express exactly the same HS-AD results, as they are interrelated by TS, and the specific weight of reactor content (ρ_{Global}) and aqueous solvent ($\rho_{Solvent}$ = 1000 kg/m^3). The NH_3 half-inhibition constant for acetoclastic methanogens ($K_{i,Snh3,Xac}$) was 0.0018 kmol N/m^3.

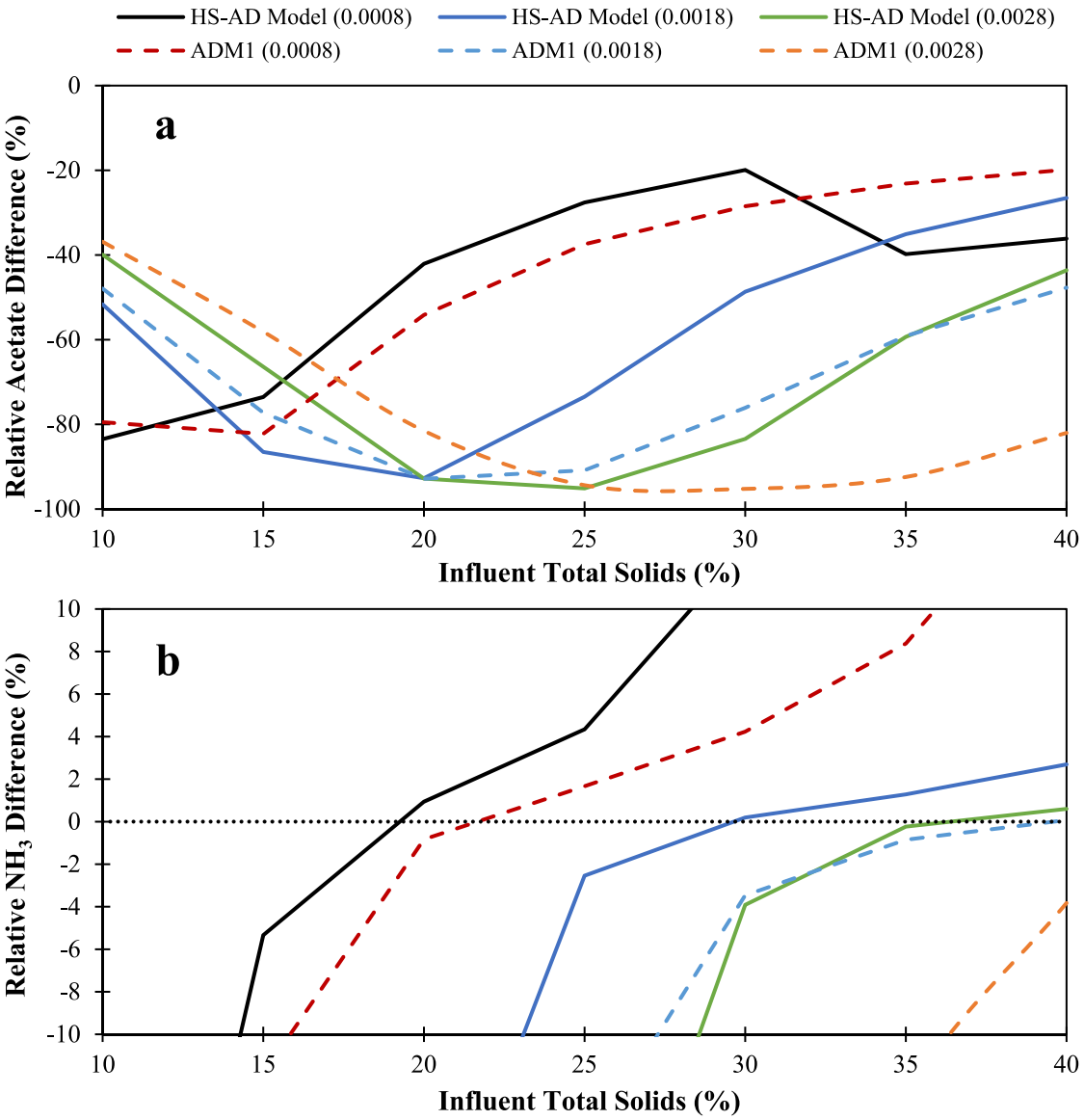

Figure 3: Contour plots for the relative difference between the 'ideal' and 'non-ideal' implementations of both ADM1 and the HS-AD model at different influent total solid (TS) contents: a) Acetate (S_{ac}) difference [Equation 14]; and b) NH_3 (S_{nh3}) difference [Equation 15].

NOTE: Values in parentheses show the NH_3 half-inhibition constants used for acetoclastic methanogens ($K_{i,Snh3,Xac}$, kmol N/m^3). Positive values over the 'inversion' threshold in panel b represent the influent TS at which the steady-state NH_3 concentration is higher for the 'non-ideal' than for the 'ideal' model implementation.

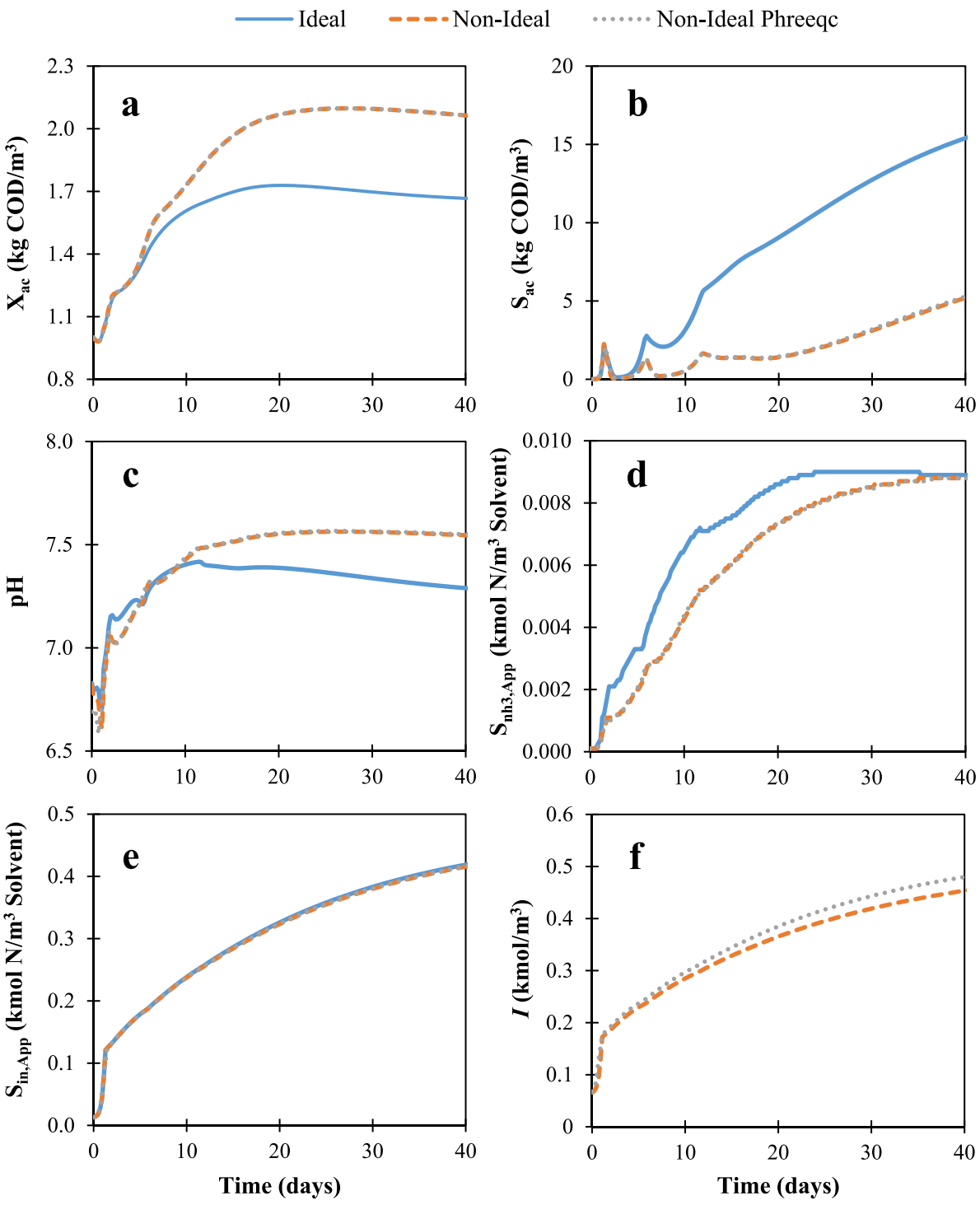

Figure 4: Effect of 'non-ideality' during the initial 40 days of HS-AD model simulations at 30 % influent TS. Comparison between 'ideal' and 'non-ideal' conditions, including the Phreeqc engine: a) Acetoclastic methanogens concentration (X_{ac}); b) total acetate concentration (S_{ac}); c) pH; d) apparent NH_3 concentration ($S_{nh3,App}$); e) total ammonia nitrogen concentration ($S_{in,App}$); and f) ionic strength (*I*).

NOTE: The NH_3 half-inhibition constant for acetoclastic methanogens ($K_{i,Snh3,Xac}$) was 0.0018 kmol N/m^3.

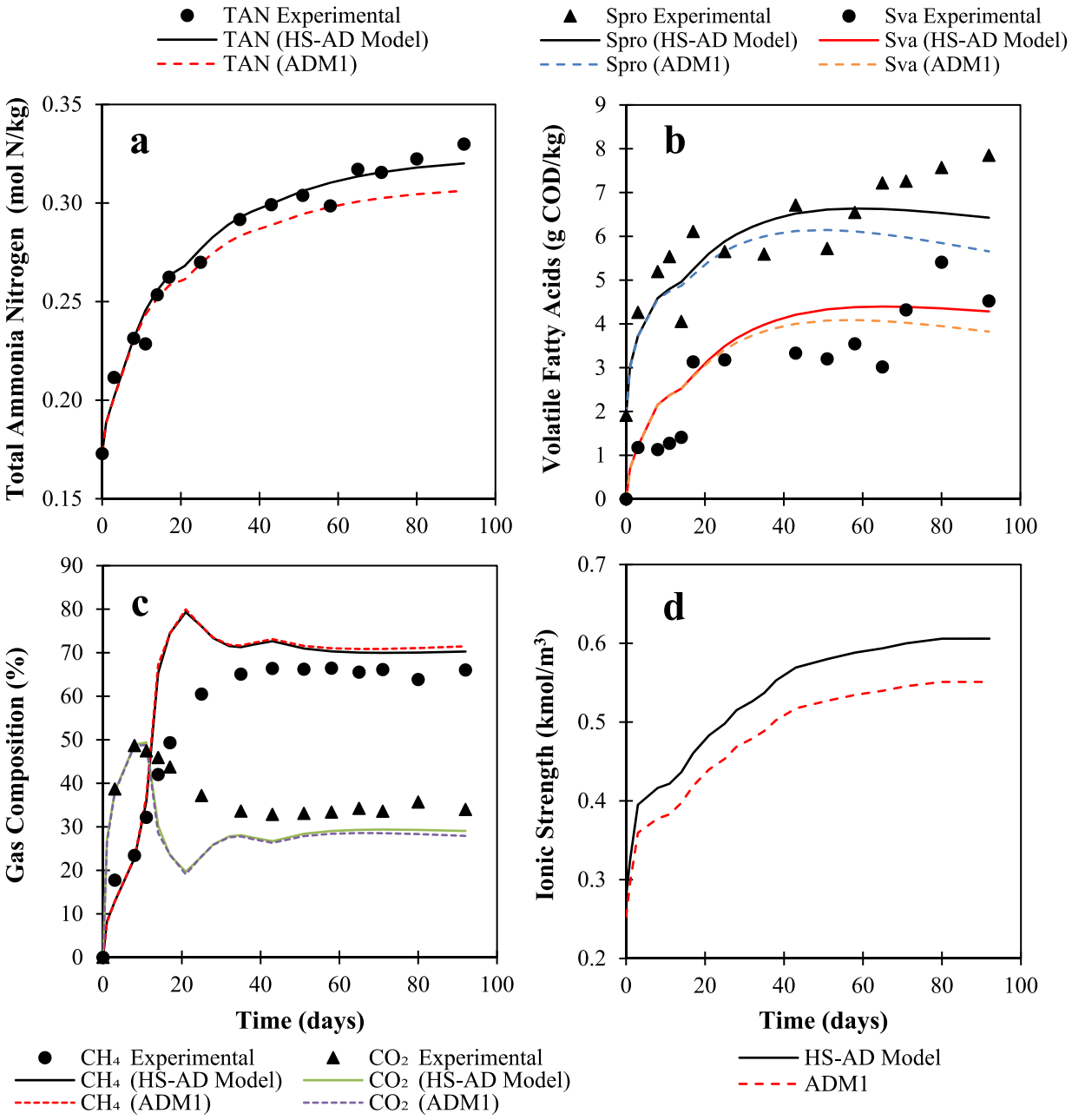

Figure 5: Model calibration results. Comparison between ADM1 Non-Ideal and HS-AD Model Non-Ideal: a) Total ammonia nitrogen (TAN); b) total propionate (S_{pro}) and valerate (S_{va}) concentrations; c) gas composition; and d) ionic strength.

Table 1: Biochemical rates used for model implementation verification and model calibration.

Process	Rate (r_j, kg COD m^{-3} d^{-1})	
	Verification	**Calibration**
Disintegration	$k_{dis} \cdot X_c$	-
Hydrolysis of Carbohydrates	$k_{h,ch} \cdot X_{ch}$	$k_{h,ch} \cdot X_{ch}$
Hydrolysis of Proteins	$k_{h,pr} \cdot X_{pr}$	$k_{h,pr} \cdot X_{pr}$
Hydrolysis of Lipids	$k_{h,li} \cdot X_{li}$	$k_{h,li} \cdot X_{li}$
Sugars Uptake	$k_{m,su} \cdot S_{su,App}/(K_{S,Xsu}+S_{su,App}) \cdot X_{su} \cdot I_{pH} \cdot I_{in}$	$k_{m,su} \cdot S_{su,App}/(K_{S,Xsu}+S_{su,App}) \cdot X_{su} \cdot I_{pH} \cdot I_{in}$
Aminoacids Uptake	$k_{m,aa} \cdot S_{aa,App}/(K_{S,Xaa}+S_{aa,App}) \cdot X_{aa} \cdot I_{pH} \cdot I_{in}$	$k_{m,aa} \cdot S_{aa,App}/(K_{S,Xaa}+S_{aa,App}) \cdot X_{aa} \cdot I_{pH} \cdot I_{in}$
LCFA Uptake	$k_{m,fa} \cdot S_{fa}/(K_{S,Xfa}+S_{fa}) \cdot X_{fa} \cdot I_{pH} \cdot I_{in} \cdot I_{h2}$	$k_{m,fa} \cdot S_{fa}/(K_{S,Xfa}+S_{fa}) \cdot X_{fa} \cdot I_{pH} \cdot I_{in} \cdot I_{h2}$
Valerate Uptake	$k_{m,c4} \cdot S_{va,App}/(K_{S,Xc4}+S_{va,App}) \cdot X_{c4} \cdot S_{va,App}/(1+S_{bu,App}+10^{-6}) \cdot I_{pH} \cdot I_{in} \cdot I_{h2}$	$k_{m,c5} \cdot S_{va,App}/(K_{S,Xc5}+S_{va,App}) \cdot X_{c5} \cdot I_{pH} \cdot I_{in} \cdot I_{h2} \cdot I_{nh3}$
Butyrate Uptake	$k_{m,c4} \cdot S_{bu,App}/(K_{S,Xc4}+S_{bu,App}) \cdot X_{c4} \cdot S_{bu,App}/(1+S_{bu,App}+10^{-6}) \cdot I_{pH} \cdot I_{in} \cdot I_{h2}$	$k_{m,c4} \cdot S_{bu,App}/(K_{S,Xc4}+S_{bu,App}) \cdot X_{c4} \cdot I_{pH} \cdot I_{in} \cdot I_{h2}$
Propionate Uptake	$k_{m,pro} \cdot S_{pro,App}/(K_{S,Xpro}+S_{pro,App}) \cdot X_{pro} \cdot I_{pH} \cdot I_{in} \cdot I_{h2}$	$k_{m,pro} \cdot S_{pro,App}/(K_{S,Xpro}+S_{pro,App}) \cdot X_{pro} \cdot I_{pH} \cdot I_{in} \cdot I_{h2} \cdot I_{nh3}$
Acetate Uptake	$k_{m,ac} \cdot S_{acApp}/(K_{S,Xac}+S_{ac,App}) \cdot X_{ac} \cdot I_{pH} \cdot I_{in} \cdot I_{nh3}$	$k_{m,ac} \cdot S_{ac,App}/(K_{S,Xac}+S_{ac,App}) \cdot X_{ac} \cdot I_{pH} \cdot I_{in} \cdot I_{nh3}$
Hydrogen Uptake	$k_{m,h2} \cdot S_{h2,App}/(K_{S,Xh2}+S_{h2,App}) \cdot X_{h2} \cdot I_{pH} \cdot I_{in}$	$k_{m,h2} \cdot S_{h2,App}/(K_{S,Xh2}+S_{h2,App}) \cdot X_{h2} \cdot I_{pH} \cdot I_{in}$
Sugar Degraders Decay	$k_d \cdot X_{su}$	$k_d \cdot X_{su}$
Aminoacids Degraders Decay	$k_d \cdot X_{aa}$	$k_d \cdot X_{aa}$
LCFA Degraders Decay	$k_d \cdot X_{fa}$	$k_d \cdot X_{fa}$
Valerate Degraders Decay	-	$k_d \cdot X_{c5}$
Butyrate Degraders Decay	$k_d \cdot X_{c4}$	$k_d \cdot X_{c4}$
Propionate Degraders Decay	$k_d \cdot X_{pro}$	$k_d \cdot X_{pro}$
Acetate Degraders Decay	$k_d \cdot X_{ac}$	$k_d \cdot X_{ac}$
Hydrogen Degraders Decay	$k_d \cdot X_{h2}$	$k_d \cdot X_{h2}$

with
$$I_{in} = S_{in,App}/(K_{i,Sin,App}+S_{in,App})$$
$$I_{h2} = K_{i,Sh2}/(K_{i,Sh2} + S_{h2,App})$$
$$I_{pH} = K_{pH}\text{^}N_{pH}/(K_{pH}\text{^}N_{pH} + S_{h+}\text{^}N_{pH})$$
$$I_{nh3} = K_{i,Snh3}/(K_{i,Snh3} + S_{nh3,App})$$

Table 2: Biochemical parameters modified for model calibration at thermophilic (55ºC) conditions.

Parameter	ADM1	This Study	Units
$k_{h,ch}$	10	0.05	d^{-1}
$k_{h,pr}$	10	0.05	d^{-1}
$k_{h,li}$	10	0.07	d^{-1}
$k_{m,su}$	70	35	d^{-1}
$k_{m,fa}$	10	4	d^{-1}
$k_{m,c5}$	30	8	d^{-1}
$k_{m,c4}$	30	8	d^{-1}
$k_{m,pro}$	20	10	d^{-1}
$K_{i,Snh3,Xc5}$	-	0.006	kmol N m^{-3}
$K_{i,Snh3,Xpro}$	-	0.006	kmol N m^{-3}
$pH_{LL,ac}$	6	5.6	
$pH_{UL,ac}$	7	6.6	
$f_{bu,su}$	0.13	0.37	
$f_{pro,su}$	0.27	0.11	
$f_{ac,su}$	0.41	0.40	
$f_{h2,su}$	0.19	0.12	
$N_{i,subs}$	-	0.001	kmol N m^{-3}

Table 3: Summary of steady-state results (i.e. day 365) for model implementation verification at different influent total solid (TS) contents.

Variable	ADM1 + Ideal Conditions			ADM1 + Non-Ideal Conditions			HS-AD Model + Ideal Conditions						HS-AD Model + Non-Ideal Conditions						Units
	10%TS	20%TS	30%TS	10%TS	20%TS	30%TS	10%TS		20%TS		30%TS		10%TS		20%TS		30%TS		
							Global	Apparent	Global	Apparent	Global	Apparent	Global	Apparent	Global	Apparent	Global	Apparent	
TS	10.0	20.0	30.0	10.0	20.0	30.0	8.3		17.2		26.5		8.3		17.1		26.4		%
TS_{Recalc}	9.1	18.4	27.5	9.1	18.5	27.8	7.4		15.5		23.8		7.4		15.6		23.9		%
$Q_{Effluent}$	170	170	170	170	170	170	168		166		164		168		166		163		$m^3\ d^{-1}$
V_{Global}	3400	3400	3400	3400	3400	3400	3400		3400		3399		3400		3400		3399		m^3
ρ_{Global}	1050	1080	1100	1050	1080	1100	1044		1069		1086		1044		1069		1086		$kg\ m^{-3}$
OLR	4.7	9.2	13.8	4.7	9.2	13.8	4.7		9.2		13.8		4.7		9.2		13.8		$kg\ COD\ m^{-3}\ d^{-1}$
HRT	20.0	20.0	20.0	20.0	20.0	20.0	20.0		20.0		20.0		20.0		20.0		20.0		d
Q_g	3224	6043	8426	3212	6307	9189	3229		5879		8203		3218		6314		8816		$Nm^3\ d^{-1}$
$\%CH_4$	57.3	55.6	53.1	57.7	57.6	56.7	57.3		54.3		51.8		57.6		57.4		54.9		%
$\%CO_2$	37.5	39.5	42.1	37.1	37.5	38.5	37.6		40.7		43.4		37.2		37.7		40.4		%
pH	7.42	7.49	7.33	7.31	7.50	7.55	7.44		7.44		7.22		7.33		7.55		7.49		
I	-	-	-	0.166	0.278	0.390	-		-		-		0.176		0.321		0.512		$kmol\ m^{-3}$
S_{ac}	0.165	4.570	15.128	0.086	0.327	3.618	0.182	0.190	7.371	8.328	19.490	24.426	0.088	0.092	0.537	0.606	10.002	12.516	$kg\ COD\ m^{-3}$
S_{in}	0.129	0.246	0.365	0.129	0.245	0.363	0.130	0.136	0.253	0.286	0.381	0.477	0.130	0.136	0.252	0.285	0.379	0.475	$kmole\ N\ m^{-3}$
S_{nh3}	0.00362	0.00820	0.00839	0.00196	0.00527	0.00810	0.00387	0.00404	0.00755	0.00853	0.00692	0.00867	0.00207	0.00216	0.00588	0.00663	0.00693	0.00868	$kmole\ N\ m^{-3}$
S_{ic}	0.153	0.199	0.154	0.158	0.267	0.330	0.154	0.161	0.162	0.183	0.102	0.128	0.160	0.167	0.269	0.304	0.246	0.308	$kmole\ C\ m^{-3}$
S_{co2}	0.01100	0.01216	0.01347	0.01048	0.01089	0.01140	0.01055	0.01102	0.01107	0.01250	0.01104	0.01384	0.01002	0.01047	0.00960	0.01084	0.00924	0.01156	$kmole\ C\ m^{-3}$
X_{ac}	0.78	1.36	1.73	0.78	1.52	2.14	0.78		1.29		1.65		0.79		1.54		1.99		$kg\ COD\ m^{-3}$
$X_{biomass}$	3.77	7.21	10.42	3.77	7.36	10.85	3.81		7.25		10.58		3.81		7.50		10.94		$kg\ COD\ m^{-3}$

NOTE: Both the ADM1 and the HS-AD model results are shown for 'ideal' and 'non-ideal' conditions. The NH_3 half-inhibition constant for acetoclastic methanogens ($K_{i,Snh3,Xac}$) was 0.0018 kmol N/m^3. The global and apparent concentrations are interrelated by the TS, and the specific weight of reactor content (ρ_{Global}) and aqueous solvent ($\rho_{Solvent}$ = 1000 $kg\ m^{-3}$).

HIGH-SOLIDS ANAEROBIC DIGESTION

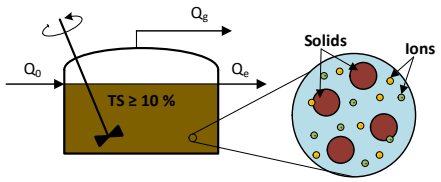

$$Apparent\ Conc. = \frac{Global\ Conc.}{1 - TS}$$

$$Ionic\ Strength = \frac{1}{2}\sum(Ion\ Conc.) \cdot (Ion\ Charge)^2$$

HS-AD MODEL SIMULATIONS

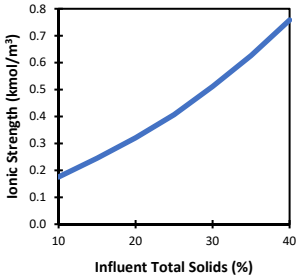

MAIN EFFECTS ON

- pH calculations;
- CO_2 transfer;
- NH_3 Inhibition;
- VFA Accumulation;
- Model Calibration.